The Helix-Coil Kinetics of a Heteropeptide

Peggy A. Thompson,† Victor Muñoz, Gouri S. Jas, Eric R. Henry, William A. Eaton, and James Hofrichter*

Laboratory of Chemical Physics, Building 5, National Institutes of Health, Bethesda, Maryland 20892-0520

Received: January 25, 1999

We have measured the kinetics of the helix-coil transition for the synthetic 21-residue peptide Ac-WAAAH$^+$-(AAAR$^+$A)$_3$A-NH$_2$ initiated by nanosecond laser temperature jumps. This peptide was designed with tryptophan in position 1 and histidine in position 5 so that the side chains interact when the backbone of residues 1−5 is α-helical. Histidine, when protonated, efficiently quenches tryptophan fluorescence providing a probe for the presence of helical structure. The kinetics measured throughout the melting transition are well-described by a single-exponential relaxation, with a rate of 3.3×10^6 s^{-1} at 301 K, the midpoint of the helix−coil transition. The rate increases with increasing temperature with an apparent activation energy of approximately 8 kcal/mol. To interpret these results we have fitted the equilibrium and kinetic data with the statistical mechanical model of Muñoz et al. (*Proc. Natl. Acad. Sci. U.S.A.* **1998**, *95*, 5872−5879). This model includes both variable helix propensities and side chain−side chain interactions. The model accounts for the single-exponential kinetics by predicting that approximately 90% of the change in the tryptophan fluorescence results from melting of stretches of helix which include residues 1−5 by passage over a nucleation free energy barrier. The measured temperature dependence is reproduced by introducing damping from solvent friction and an activation barrier for the individual helix propagation and melting steps. This barrier is somewhat larger than that which results from the loss in conformational entropy or breaking of hydrogen bonds. The model provides a description of the kinetics of the helix-coil transition which is consistent with the results of other experimental studies as well as molecular dynamics simulations.

Introduction

The formation of α-helices is one of the fundamental processes in protein folding.[1] It is now possible to study the kinetics of the helix-coil transition in peptides which have lengths and compositions comparable to those of helical segments of proteins. This has been made possible by the discovery that alanine-based peptides form stable helices in solution,[2,3] by a theoretically based analysis of helix propensities[4,5] and by the application of laser-induced temperature jump methods.[6−9] In a previous study, using an artificial fluorescent probe at the N-terminus of an alanine-based peptide, we found that the kinetic amplitudes could not be explained by a classical nucleation-growth model. This motivated the present study in which tryptophan and histidine were inserted into the same peptide to provide an intrinsic fluorescence probe. To interpret the results obtained for this peptide, the nucleation-growth description has been expanded to include side-chain interactions and variable helix propensities.[1] This model successfully explains the kinetics of both the previous homopolypeptide and our designed heteropeptide. We obtain rates for the individual helix propagation steps from the analysis which, together with the measured rates for the overall helix-coil kinetics, provide useful benchmarks for all-atom molecular dynamics simulations.

In statistical mechanical descriptions of the helix-coil transition,[10−12] two distinct processes occur when the helical state is stabilized or destabilized. First, peptides gain or lose helices by passing over the (nucleation) free energy barrier which separates states with extended stretches of helix from those which have only a few scattered helical residues. This barrier is very asymmetric. The coil side of the barrier, which arises from the loss of conformational entropy associated with fixing peptides in helical conformations without formation of any compensating stabilizing interactions (i.e., hydrogen bonds and $i,i+4$ interactions between backbone and C_α atoms),[1,3,10] is quite steep. On the helix side of the barrier, the slope is more gentle because it is determined by the small difference between the entropy loss and the free energy change which results from these stabilizing interactions. Because of the small incremental free energy change, a relatively large number of helical residues ($\gtrsim$10) are needed to compensate for the nucleation free energy and produce stable helical peptides.

More than 20 years ago, kinetic models based on this picture were developed to interpret relaxation experiments on long polypeptides[13] and the results of these early studies have been summarized by Grunewald et al.[14] The nucleation barrier is significantly larger than those for more localized changes in helical structure so the gain or loss of helical sequences is expected to be the slowest process in helix formation. In the analytical formulation of Schwarz,[13] the average relaxation time for forming or melting helices is related to the average time for helix elongation by a factor of $(2\sigma)^{-1}$, where σ, the equilibrium constant for formation of the nucleus, is estimated as 10^{-2}−10^{-3} from equilibrium studies.[2−5] It is important to recognize that this barrier produces the slowest relaxation when helices are melted as well as when they are formed because, in experiments performed near the midpoint of the melting transition, the total height of this barrier relative to both the coil states and occupied helical states is nearly the same. When the nucleation barrier is sufficiently large, the system becomes effectively two-state (peptides are either *all-coil* or *all-*

* To whom correspondence should be addressed.
† Current address: Biopraxis, Inc., 10655 Sorrento Valley Rd., Suite 200, San Diego, CA 92121.

10.1021/jp990292u
Published on Web 12/22/1999

helix) and crossing this barrier is the only observed process. When the nucleation barrier is smaller, a change in helix stability alters not only the *number* but also the *length* of helical sequences.[10−13] Because this slope on the helix side of the barrier is small and helical residues can be added and removed rapidly compared to the rate for crossing the nucleation barrier, peptides which contain helices reequilibrate to the new equilibrium distribution of lengths on a time scale which is significantly faster than equilibration with the all-coil state.[9,13]

Recent kinetic studies[6,8,9] of the helix-coil transition of an alanine peptide using nanosecond temperature jumps have provided support for this picture. In the first study, Williams et al.[6] measured absorbance changes in the amide-I region to monitor formation of α-helical hydrogen bonds. A single relaxation with a relaxation time of about 200 ns was observed. In the second study, we measured the kinetics for a similar peptide, probed by fluorescence changes in an N-terminal probe, methylaminobenzoic acid (MABA), and observed a much faster relaxation at about 20 ns.[8,9] In an effort to reconcile these apparently discrepant observations, we developed a simplified model of the helix-coil kinetics which we called a "kinetic zipper" model. This model showed that the process of forming and melting helical sequences appeared as the slowest relaxation, well separated from other more rapid processes. The process of "zipping" and "unzipping" the helical sequence appeared as a cluster of relaxations, having rates which differed by less than a factor of 3. These relaxations could be fitted to within 1% accuracy by a single-exponential relaxation.[9] The model thus provided a reasonable explanation for the two experimentally observed relaxation times which is consistent with the equilibrium picture.[10−12]

Our model further showed that the amplitude for the fast relaxation of the N-terminal helix content was significantly larger than the corresponding amplitude for the average helix content. This prediction is qualitatively consistent with the observed amplitudes, but problems arose when we attempted to use the predictions of the model quantitatively. The prediction that about half the amplitude for an N-terminal probe should be slow was inconsistent with the data, which exhibited no slow phase (<10%). What is the reason for this discrepancy? Is it because MABA is sufficiently different from alanine that our assumption that this peptide could be modeled as a homopolymer did not hold or is there a more fundamental problem with the model which makes it unsuitable for quantitative predictions?

To address these questions, we have extended our original observations by utilizing an improved probe for helix formation at the N-terminus. We designed a peptide, Ac−WAAAH$^+$-(AAAR$^+$A)$_3$A-NH$_2$ (Figure 1), which we shall refer to as W_1H_5-21, in which helix formation can be monitored by observing changes in tryptophan fluorescence. The basic feature of the design is that the side chains of tryptophan and histidine spatially interact in the α-helical structure (an $i,i+4$ interaction). When the histidine is protonated, this interaction contributes significantly to the stability of the helix[4,5,15,16] and also significantly quenches the fluorescence, providing an intrinsic probe of helix formation.[16−18] The favorable interaction compensates to some degree for the lower helix propensities of tryptophan and histidine,[4,5] producing a peptide which is more than 80% helical at 273 K. A repulsive interaction between the protonated histidine in position 5 and the arginine in position 9 is also introduced when the residues 5−9 are helical. There are several obvious advantages to using such an intrinsic probe. It can be readily incorporated in peptide synthesis, permitting almost complete flexibility in the positioning of the probe. In addition,

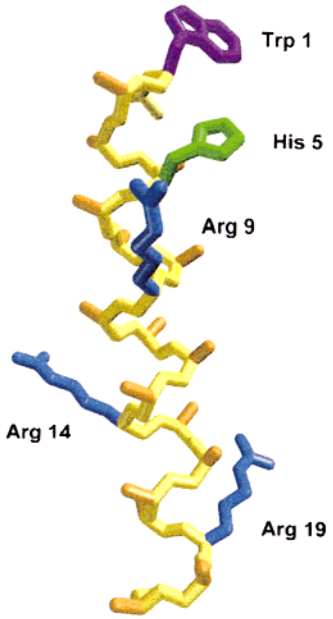

Figure 1. Fully helical form of W_1H_5-21. The tryptophan (purple) side chain acts as a fluorescent probe. It interacts with the protonated histidine (green) side chain when these residues are helical and electron transfer to the histidine quenches the tryptophan fluorescence. The arginine (blue) side chains are included to increase peptide solubility, while the alanine (orange) side chains are included to stabilize the helical conformation of the peptide.

a large body of data already exists on the effects of individual amino acids on helix stability.[2−5] These data provide a basis for intelligent design of stable peptides, as well as the opportunity to tailor the properties of the probe (e.g. by varying its stability).

The high stability of the helical form of this peptide, together with the relatively low cooperativity of the helix-coil transition, permitted the kinetics to be measured over a relatively wide range of temperatures (275−350 K). The melting kinetics exhibit an unexpectedly large temperature dependence, with an apparent activation energy of about 8 kcal/mol. To interpret these results we have used a modified version of the statistical mechanical model developed by Muñoz et al.[1] to describe the formation of a β hairpin. The model can be readily used to describe the kinetics of the helix-coil transition. It includes sequence heterogeneity, which produces positional variations in helix propensity and hence position-dependent nucleation and growth rates, as well as specific interactions between side chains in the helical conformation, which produces position-dependent melting rates. This model is able to describe the observed rates and amplitudes with sufficient precision that we are able to obtain specific information about both the nucleation free energy barrier and the rates of helix elongation.

Experimental Section

Materials. *N*-acetyl-L-tryptophanamide (NATA) was purchased from Sigma. The peptides were either synthesized using an Applied Biosystems 431A peptide synthesizer or purchased from California Peptide Research, Inc. As determined from HPLC, the purity was greater than 95%. The molecular structure of the 21-residue peptide is shown in Figure 1. The N-terminus of the peptide is acetylated and the C-terminus amidated, so the peptide actually contains 22 peptide bonds and the N-terminal tryptophan, which is associated with the second peptide bond, becomes residue 2 in our model.

Equilibrium Experiments. To ensure that the side chain of histidine was protonated, peptide solutions were prepared in 20 mM acetate buffer, pH 4.9. Fluorescence emission measurements (excitation at 264 nm) were made with a SPEX Fluorolog spectrofluorimeter using peptide concentrations of 4−8 μM. The emission quantum yields were determined relative to NATA at pH = 6.9 (Φ_f = 0.14 at 293 K). Circular dichroism spectra were measured on a JASCO 710 spectropolarimeter using a 0.5 mm path length cylindrical cell and concentrations of ~0.1 mM. Peptide concentrations were determined from the absorbance of tryptophan at 280 nm using an extinction coefficient of 5690 M^{-1} cm^{-1}.[19]

Analysis of Equilibrium Experiments. We fitted the measured ellipticity at 222 nm to obtain parameters for use in modeling the kinetics. To fit the CD data, we used expressions for the mean residue molar ellipticity which are similar to those proposed by Scholtz et al.[20] and modified for tryptophan-containing peptides by Chakrabartty et al.[21] The ellipticity of a species containing a contiguous sequence of j helical residues which begins at residue i is given by

$$\theta_{j,i} = (j - n_\alpha)(\theta_\alpha + \theta_{\alpha T}(T-T_0)) + \delta_{1,i}\theta_{\alpha W} \quad \text{helical residues}$$
$$+ (n - j)(\theta_r + \theta_{rT}(T-T_0)) + (1 - \delta_{1,i})\theta_{rW} \quad \text{coil residues} \tag{1}$$

where n is the length of the peptide, T_0 is 273 K, $\theta_\alpha + \theta_{\alpha T}(T-T_0)$ is the molar ellipticity of the peptide backbone of each residue in an infinite helix at temperature T, $\theta_{\alpha W}$ is the side-chain contribution of tryptophan in a helix, and $\delta_{1,i}$ is an index, the value of which is 1 if the N-terminal tryptophan is included in the helical sequence and 0 otherwise; $\theta_r + \theta_{rT}(T-T_0)$ and θ_{rW} are the corresponding properties for the random coil state. The empirical parameter, n_α, is introduced to account for the fact that the mean-residue ellipticity is length dependent[22−24] and is conventionally given a value of about 2.5 based on the work of Chen et al.[25] (Note that this procedure assigns no 222 nm CD to the first n_α residues of a helical sequence; while short helices are predicted to contribute to the ellipticity[23,24] the populations of such short helical sequences are small, so the calculated CD is nearly independent of the CD amplitude assigned to these species.) To calculate the ellipticity of each species within our ensemble, the ellipticity of the j helical residues, calculated from the first line of eq 1, is added to the contribution of the $n-j$ coil residues, calculated from the second line. The total ellipticity is then straightforwardly calculated as

$$[\theta]_{222}^{obs} = P_{0,0}\theta_{0,0} + \sum_{j=1}^{n}\sum_{i=1}^{n-j+1} P_{j,i}\theta_{j,i} \tag{2}$$

where $P_{0,0}$ is the fractional population of the all-coil state and $P_{i,j}$ is the fractional population of the species having j helical peptide bonds in a sequence which begins at peptide bond i.[1] In carrying out the fit, we have found it useful to vary the six ellipticity parameters in eq 1 (θ_α, $\theta_{\alpha T}$, $\theta_{\alpha W}$, θ_r, θ_{rT}, and θ_{rW}) as well as n_α. We have constrained these parameters to lie within bounds determined by extensive experimental and theoretical investigations.[26]

There is, to our knowledge, no universally accepted model which describes the quantum yield of tryptophan fluorescence in peptides and proteins. Nonetheless, we need a model that can quantitatively describe the temperature-dependent quantum yield to analyze both our equilibrium and kinetic data. In developing a working model we have begun with the analysis of the pH and temperature dependence of the lifetimes of tryptophan and indole by Robbins et al. (1980).[27] These authors describe their lifetime data using three quenching processes. One is intersystem crossing to the triplet state; the second involves internal proton transfer and is responsible for the decrease in the quantum yield of NATA when the pH is reduced from 11 to 7; the third is electron transfer from the indole excited state to water. In their model, the radiative rate, k_f, and the rate of intersystem crossing k_t, are temperature-independent with values of k_f =5.0 × 10^7 s^{-1} and k_t = 3.3 × 10^7 s^{-1} for tryptophan at pH 11. The electron transfer rate, $k_{e_{aq}^-}$ is highly temperature dependent and is primarily responsible for the fact that the quantum yield of tryptophan decreases monotonically with temperature; it is therefore described as an activated process

$$k_{e_{aq}} = k_{e_{aq}}^0 \exp\left(-\frac{\Delta E_{e_{aq}}}{RT}\right) \tag{3}$$

where $k_{e_{aq}}{}^0 \approx 5 \times 10^{16}$ s^{-1}, $\Delta E_{e_{aq}} \approx 12$ kcal/mol. The intramolecular quenching (proton transfer) rate, k_i, is described by the weakly temperature-dependent expression

$$k_i = k_i{}^0 \frac{T}{\eta(T)} \tag{4}$$

where $k_i{}^0 \cong 6.8 \times 10^5$ cP K^{-1} s^{-1} and $\eta(T)$ is the solvent viscosity. The quantum yield is then given by

$$\Phi = \frac{k_f}{k_f + k_t + k_i + k_{e_{aq}}} \tag{5}$$

This expression should provide a reasonably good description of the quantum yield of states in which the tryptophan is a coil residue. It clearly must be modified under conditions where tryptophan is partially or fully shielded from water since the electron transfer rate must decrease. Moreover, when the $W-H^+$ interaction is formed, there is at least one additional quenching process which might occur via either a proton transfer or an electron transfer mechanism. The data of Steiner and Kirby[18] show that the quenching rate for tryptophan in solution by a wide range of compounds, including histidine, is highly correlated with the rate of electron capture, suggesting that quenching probably occurs via electron transfer. If we assume that this is the mechanism, then the rate of this process should be described by

$$k_{e_{WH}} = k_{e_{WH}}^0 \exp\left(-\frac{\Delta E_{e_{WH}}}{RT}\right) \tag{6}$$

To simplify fitting the quantum yield data, we have used a reduced form of eq 5 that includes a single temperature-independent quenching rate k, which effectively represents the sum ($k_t + k_i$), and a temperature-dependent rate, described by $Ae^{-E/RT}$, which describes the electron transfer processes, for each set of conditions. We shall refer to states in which the $W-H^+$ interaction is present in the helical sequence ($i \le 2$; $i + j \ge 6$) as (+), and those in which the $W-H^+$ interaction is not present as (−). The quantum yield for these states is then given by

$$\Phi_\pm = \frac{k_f}{k_f + k_\pm + A_\pm e^{-E_\pm/RT}} \tag{7}$$

The total quantum yield is given by

$$\Phi_{obs} = \sum_{i=1}^{2}\sum_{i+j=6}^{n} P_{j,i}\Phi_{+} + (1 - \sum_{i=1}^{2}\sum_{i+j=6}^{n} P_{j,i})\Phi_{-} \qquad (8)$$

This description requires a total of only three free parameters to describe the temperature-dependent quantum yields of each state, capturing most of the photophysics of the quenching of tryptophan fluorescence using no more parameters than would a quadratic polynomial.[28]

Temperature Jump Experiments. Temperature jumps of 10−20 K were generated by absorption of a near-infrared laser pulse (1.54 μm) by the aqueous solution. The time dependence of the fluorescence intensity was monitored to measure the kinetics. Tryptophan was excited using a continuous ultraviolet probe beam (264 nm) and the emitted light was monitored using band-pass filters which transmitted wavelengths from 320 to 400 nm. The kinetic experiments were carried out in an 0.05 × 1.0 cm fluorescence cuvette at concentrations of 0.5−0.8 mM.

The temperature jump instrument has been previously described in detail.[8,9] The basic approach is to use a pulse from a Q-switched Nd:YAG laser (1064 nm) which has been Raman shifted in methane to a wavelength of 1.54 μm to produce the temperature jump, a continuous ultraviolet probe beam to excite tryptophan fluorescence, and a photomultiplier and a transient digitizer to record the emitted light. Our apparatus differed in three details from that described earlier.[8,9] First, the 1.54 μm light pulse was split into two equal intensity beams using a 50:50 beam splitter and focused onto the same spot from opposite sides of the sample cuvette to obtain more uniform heating. Second, to minimize tryptophan photodamage by the 264 nm probe beam a shutter was introduced which minimized the time during which the sample was exposed to ultraviolet radiation. The emitted light, collected at 90° to the excitation beam, was detected with an end-on photomultiplier tube (Hamamatsu R6427) in place of the 1P28 used previously.

Kinetic Modeling. The original "kinetic zipper" model,[9] was developed in an effort to understand qualitative features of the helix-coil kinetics and was formulated for a homopolypeptide. This was a reasonable approximation for a peptide comprised only of alanine and arginine, since the helix propensities for these two residues differ by only about 0.1 kT.[4,5] In the present peptide (Figure 1), W_1H_5-21, the free energy necessary to constrain the tryptophan and histidine into helical dihedral angles, differs from that for alanine and arginine by about kT,[4,5] so it is unrealistic to attempt to understand the peptide dynamics without accounting for the sequence heterogeneity. Modeling W_1H_5-21 also requires the introduction of specific side chain interactions to account for the stabilizing interaction between W_1 and H_5^+ and the repulsive interaction between H_5^+ and R_9^+.

A model which includes these effects has been developed by Muñoz et al. to analyze the folding of a β hairpin peptide.[1,29] Species are identified by the conformation of the CONH peptide bonds, defined by the values of the flanking dihedral angle pairs (ψ of residue i and ϕ of residue $i + 1$). Proceeding from the N-terminus, ψ_i determines the orientation of the peptide connecting residues i and $i + 1$ and ϕ_{i+1} determines the orientation of the C_α-C_β bond of residue $i + 1$ in the sequence. We consider only two states for each peptide bond—native (i.e., helical dihedral angles for ψ_i and ϕ_{i+1}) denoted h, and nonnative (i.e., nonhelical values for one or both of ψ_i and ϕ_{i+1}), denoted c. In the absence of stabilizing interactions, the c state is favored because its conformational entropy is higher than that of the native state. For a peptide with n amino acid residues, acetylated at the N-terminus and amidated at the C terminus, there are $n + 1$ peptide bonds and 2^{n+1} possible conformations. Because the N-terminal peptide bond is formed by the acetylated amino group W_1 is the side chain between the first and second peptide bonds in our model.

To simplify the model, it is assumed that interactions between two residues of the peptide (i.e., backbone hydrogen bonds or side chain interactions) occur only if all intervening peptide bonds have native values. A hydrogen bond between the carbonyl of residue i and the NH of residue $i + 4$ forms when the four pairs of intervening dihedral angles are helical. Fixing these four dihedral angle pairs also fixes the side chains of residues i and $i + 4$ so, if $i = 2$, the indole side chain of tryptophan forms a stabilizing interaction with the protonated imidazole side chain of histidine. The thermodynamic factors included in the model are thus ΔH_{hb}, the enthalpy change associated with stabilizing CO···HN backbone hydrogen bonds (this term also includes any other interactions between backbone atoms and the C_β of residues i and $i + 4$), a stabilizing (ΔG_{WH}) and a destabilizing (ΔG_{HR}) side chain interaction, which are assumed to be temperature-independent, and two values of ΔS_{conf}, the destabilizing entropy change which results from fixing a ψ_i,ϕ_{i+1} pair in a helical conformation ($\Delta S_{conf,A}$ for alanine and arginine and $\Delta S_{conf,W}$ for tryptophan and histidine).[30] The model does not consider the possibility of interactions between side chains of residues which are not helical.

To simplify the modeling of the kinetics, we invoke the single sequence approximation, which considers only species which contain a single stretch of contiguous helical residues. This assumption reduces the number of species from over 4 million to 254. All other species (those which contain multiple sequences of helical residues) are included in the model as a contribution to the entropy of the coil state. In these species the helical configuration of the peptide bond is designated h^* because it is assumed that no stabilizing interactions are formed for any distribution of h^* peptide bonds. Lifson and Roig[12] recognized that in α-helices, since $T\Delta S_{conf}$ is of the order of 1 kcal/mol, the population of residues in the h^* state within a stretch of coil residues is not negligible. For the all-coil state of a 21-residue alanine peptide, the magnitude of this entropy is about 5 eu. Equation 3 of Muñoz et al.,[1] which describes the weight of the coil state, must be modified for a heteropolymer in which the propensities for the native conformation are sequence-dependent. It is replaced by

$$w_{0,0} = \prod_{i=1}^{n}(1 + \exp(\Delta S_{conf,i}/R)) - \sum_{j+1}^{n}\sum_{i=1}^{n-j+1} \exp(j\Delta S_{conf,i}/R) \qquad (9)$$

where $\Delta S_{conf,i}$ is the helix entropy change for constraining peptide bond i in its helical conformation. $\Delta S_{conf,i}$ is the average of the values for residue i and residue $i + 1$. The model has been described in detail and the single sequence approximation tested by Muñoz et al.[1]

In the model of Muñoz et al.,[1,29] as in other models for the helix-coil equilibria,[4,12] the nucleation barrier results simply from the loss of the conformational entropy of three pairs of ϕ,ψ angles. Its magnitude is therefore specified by the same free energy parameters which determine the propagation equilibrium constants (in the kinetic zipper model,[9] the nucleation parameter, σ, was treated as an additional adjustable parameter). To further reduce the parameter list we adopt a simplified description of the kinetics of the $c \rightleftharpoons h$ transition. We assume that the $c \rightleftharpoons h$ transition takes place through a transition state $ch^‡$ which has a fraction λ_S of the conformational entropy of the coil and fractions λ_H and λ_G of the free energy changes for

formation of the hydrogen bond and side chain interactions.

$$c \underset{\Delta G^{\ddagger}_{hc}}{\overset{\Delta G^{\ddagger}_{ch}}{\leftrightarrows}} h \tag{10}$$

where the activation free energies are $\Delta G^{\ddagger}_{hc} = \Delta E_0 + \lambda_H \Delta H_{hb} + \lambda_G \Delta G_{sc} - \lambda_S T \Delta S_{conf}$, and $\Delta G^{\ddagger}_{ch} = \Delta E_0 - (1 - \lambda_H)\Delta H_{hb} - (1 - \lambda_G)\Delta G_{sc} + (1 - \lambda_S)T\Delta S_{conf}$. The kinetic contribution to the barrier height is described by E_0.

In describing the kinetics of the β hairpin, Muñoz et al.[1,29] chose $\lambda_S = 1$ and $\lambda_H = \lambda_G = 0$ as the values of these parameters. Our default choice for the transition state for the α-helix ($\lambda_S = 0.5$; $\lambda_H = \lambda_G = 0$) is based, in part, on the molecular mechanics studies of Brooks and co-workers[31] who investigated the path from *c* to *h* using umbrella sampling and found that the transition could be approximately described as a rotation around the ψ dihedral angle. The extended or "coil" value of ψ is about 145° and the helical value is about −45°. The maxima are found to lie approximately midway between the extended and helical values. This transition state might therefore be expected to have somewhat higher entropy than the helical state, but the large change in the value of ψ would suggest that specific interactions, such as the hydrogen bond, should be nearly absent. For this reason we have used these values in the fits and simulations described below. We assume that the rates from $c \rightarrow h$ and from $h \rightarrow c$ are described by the energy barriers defined in eq 10. The $c \rightarrow h$ rate is then given by

$$k_{c\rightarrow h} = k_0 \left(\frac{\eta_0}{\eta}\right)^{\kappa} \exp\left(-\frac{\Delta G^{\ddagger}_{ch}}{RT}\right) \tag{11}$$

and the $h \rightarrow c$ rate by

$$k_{h\rightarrow c} = k_0 \left(\frac{\eta_0}{\eta}\right)^{\kappa} \exp\left(-\frac{\Delta G^{\ddagger}_{hc}}{RT}\right) \tag{12}$$

For most of our simulations we have assumed a value for the viscosity exponent, κ, of 1.

Results and Discussion

Equilibrium Characterization of the Helix ⇌ Coil Transition. The equilibrium properties of the peptide were characterized by circular dichroism and fluorescence measurements. At low temperature, the spectra are typical of those found for α-helical peptides exhibiting minima at 208 and 222 nm and a maximum at 190 nm. When the spectra are compared through the melting curve, an isodichroic point is found at 202 nm, indicating that a population of structures other than α-helix and coil is not resolved. The molar ellipticity at the 222 nm minimum, $[\theta]_{222}$, is shown in Figure 2a. As observed for many other small helical peptides, the transition is very broad, extending over more than 70 K. The quantum yields measured for *N*-acetyltryptophan amide (NATA), the control peptides WAAA and $WAAAH^+$ and W_1H_5-21 are shown in Figure 2b. The fluorescence of both tryptophan and NATA is strongly quenched as the temperature is increased. The quantum yields of the control peptides also increase monotonically with decreasing temperature, while that of the helical peptide plateaus at a value of about 0.06 below 310 K. The quantum yields of the control peptides are somewhat smaller than NATA, but significantly larger than that of the W_1H_5-21.

The equilibrium data were simultaneously fitted by varying the values for the hydrogen bond enthalpy, ΔH_{hb}, the helix propensities $\Delta S_{conf,A}$, for alanine and arginine, and $\Delta S_{conf,W}$, for tryptophan and histidine as well as the interaction energies

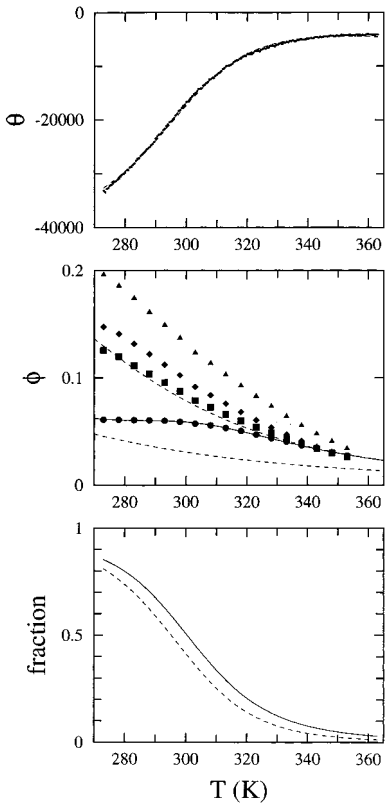

Figure 2. Equilibrium data for W_1H_5-21 as a function of temperature. (a, top) (●) molar ellipticity (per peptide bond) at 222 nm; (− − −) the fit obtained using the modified model of Muñoz et al.[1] and the equilibrium and CD parameters in Table 1. (b, middle) Fluorescence quantum yields of (●) W_1H_5-21, (◆) WAAA, (■) $WAAAH^+$, and (▲) NATA in solution. (—) The fit obtained using the model and the equilibrium and fluorescence parameters in Table 1. (− − −) The quantum yield of states which include the $W_1-H_5^+$ interaction, $\{i \leq 2, i + j \geq 6\}$ and (- - -) the quantum yield of states which do not include the $W_1-H_5^+$ interaction. (c, bottom) Helical contents calculated from the fit to the model. (—) The fraction of helical peptide bonds. (- - -) The fraction of molecules which contain the $W_1-H_5^+$ interaction.

ΔG_{WH}, between W_1 and H_5^+ and ΔG_{HR}, between H_5^+ and R_9^+. The CD data were fitted using eqs 1 and 2 and the fluorescence data using eqs 7 and 8. The seven empirical parameters in eq 1 and the six empirical parameters in eq 7 were also varied in these fits. Constraints were imposed on these parameters to ensure that the parameters remained within reasonable bounds. The fits are shown superposed on the data in Figure 2 and the fitted parameters are presented in Table 1. A remarkable success of the fitting, illustrated in Figure 2b, is the close correspondence between the calculated quantum yield of the unfolded peptide and the measured quantum yield of the reference peptide $WAAAH^+$. This result suggests that, in the unfolded peptide, quenching of tryptophan fluorescence by residues more than four residues distant in the sequence is negligible. The helix content obtained from the fit, measured both as the fraction of helical residues and as the fraction of $W_1-H_5^+$ interactions, is shown in Figure 2c. The midpoint of the melting curve for helical residues is at 301 K, and the fraction of residues which are helical increases to −85% at 273 K. The fraction of $W_1-H_5^+$ interactions exhibits temperature dependence which is very similar to that of the average helix content but its magnitude is about 10% smaller at all temperatures. Figure 2c clearly shows that a significant change in both the average helix content and the $W_1-H_5^+$ population can be achieved with temperature jumps of 10−20 K at temperatures between 270 and 340 K.

TABLE 1: Parameters from Fit to Equilibrium and Kinetic Data

Thermodynamic Parameters[a]	
$\Delta S_{conf,A}$	−2.35 cal/(mol K)
$\Delta S_{conf,W}$	−4.35 cal/(mol K)
ΔH_{hb}	−1.00 kcal/mol
ΔG_{WH}	−1.63 kcal/mol
ΔG_{HR},	+1.63 kcal/mol
Kinetic Parameters	
k_0	1.20×10^{12} s^{-1}
E_0	3.71 kcal/mol
Spectroscopic Parameters	
CD Parameters[b]	
n_α	4.10 residues
θ_α	-4.30×10^4 deg cm^2/dm
$\theta_{\alpha T}$	145 deg cm^2/(dm K)
$\theta_{\alpha W}$	-4.41×10^4 deg cm^2/dm
θ_r	600 deg cm^2/dm
θ_{rT}	−40 deg cm^2/(dm K)
θ_{rW}	-2.53×10^4 deg cm^2/dm
Fluorescence Parameters[c]	
k_-/k_f	3.42
A_-/k_f	3.74×10^4
E_-	4.99 kcal/mol
k_+/k_f	6.96
A_+/k_f	6.7×10^3
E_+	3.35 kcal/mol

[a] Thermodynamic parameters were subjected to the following constraints: $\Delta S_{conf,A} < 0$; $\Delta S_{conf,A} - \Delta S_{conf,W} < 2$; $-0.8 > \Delta H_{hb} > -1.4$; $\Delta G_{WH} > -2$; $\Delta G_{WH} > \Delta G_{HR} > 0$. [b] CD parameters were subjected to the following constraints: $5 > n_\alpha > 2$; $-45000 > \theta_\alpha > -35000$; $150 > \theta_{\alpha T} > 50$; $740 > \theta_r > 540$; $-50 > \theta_{rT} > -40$; $80\,000 > \theta_{\alpha W} > -80\,000$; $0 > \theta_{rW} > -80\,000$. [c] Fluorescence parameters were subjected to the following constraints: $0 < E_+ < E_-$; $E_- - 4 < E_+$; $A_-/k_f < 10^6$; $A_+/k_f < 10^6$; $10^{-2}\, A_-/k_f < A_+/k_f < 100\, A_-/k_f$; $k_-/k_f < 6$; $k_+/k_f < 15.7$; $k_-/k_f + 10^{-4}\, A_-/k_f > 4$.

The fit produces values for the helical propensities of W_1 and H_5^+ which are similar to those obtained by substitution studies in peptides.[4,5] The magnitude of the interaction free energy between the tryptophan and charged histidine side chains, $\Delta G_{WH} = -1.6$ kcal/mol, is somewhat larger than the value obtained from the substitution studies in alanaine peptides which ranged from −0.8 to −1.2 kcal/mol, depending on the method of analysis[16] but is similar to the value of -1.3 ± 0.1 kcal/mol found for a tertiary interaction in barnase.[32] The value of +1.6 kcal/mol for the interaction free energy between H_5^+ and R_9^+ is significantly larger than that used between charged residues in positions i, i+4 in AGADIR.[4,5] The large interaction energies make it very unlikely that residues H_5^+ through R_9^+ will occur in a helical sequence which terminates to the C-terminal side of W_1. The low probability of these species is shown in Figure 3, where the equilibrium population of the 254 species is displayed at the midpoint of the melting transition (301 K). The most populated helical states contain 21 helical residues and the $W_1-H_5^+$ interaction. Long helices ($j > 17$) which do not include W_1 are unstable because they include the unfavorable $H_5^+-R_9^+$ interaction. Species which contain 16 or fewer helical residues and span only the alanine-rich C-terminal region of the peptide are also highly populated. The net result is that the $W_1-H_5^+$ interaction stabilizes the first five residues when they are helical and hence makes the fluorescence a much more faithful probe of the average helix content than might be expected for an N-terminal probe that does not interact with other residues in the helix. The results in Figure 2c reflect this effect, because the probability that W is helical is almost as large as the probability that the average residue is helical.

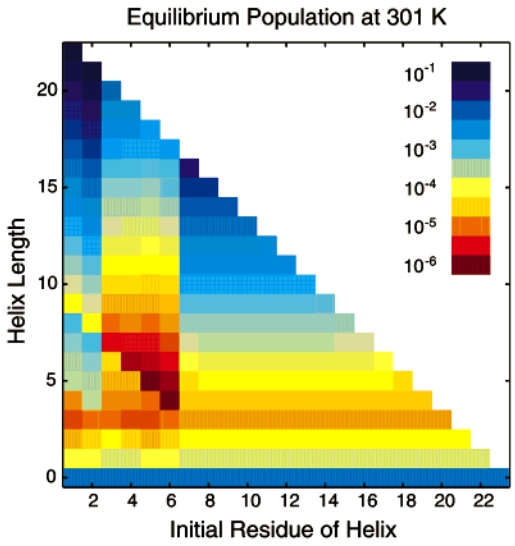

Figure 3. Populations at the midpoint of the folding transition for W_1H_5-21 at 301 K. The number of helical residues (j) is plotted on the y axis and the initial helical residue (i) is plotted on the x axis. The populations of the 254 states of the model are represented by a color code which is dependent on the logarithm of the population. The (logarithmic) color code is shown at the right of the figure. The most populated states ($p = 0.1$) are coded blue to denote low free energy and the least populated states ($p = 10^{-6}$) are coded in red to denote high free energy. The population of the $j = 0$ state has been divided by 23 and the resulting value is plotted in bins $\{j = 0; i = 1{:}23\}$.

Temperature Jump Kinetics. Laser temperature jumps to final temperatures ranging from 277 to 338 K were used to rapidly perturb the helix−coil equilibrium. Figure 4 shows examples of three kinetic measurements at final temperatures of 281, 300, and 318 K. The initial rapid decrease results from a change in the intrinsic tryptophan fluorescence due to the change in temperature. All of the relaxation data measured at times when the sample was not exposed to the near-infrared heating pulse could be fitted with a single-exponential relaxation. The dependence of the measured relaxation rates on temperature is shown in Figure 5. Most of the data exhibit small but significant deviations from a single exponential at times less than 20 ns after the beginning of the temperature jump which overlap the near-infrared excitation pulse. We have observed comparable changes in fluorescence during the excitation pulse in solutions of NATA and tryptophan, but not in dansyl. Presumably the decrease in fluorescence intensity in this time interval results from absorption of the infrared pulse by the excited singlet state of tryptophan. The population of this state could be decreased either by local heating, which increases the quenching rate, or by excitation to higher singlet states. The absence of this effect in dansyl, which has a temperature-independent quantum yield, is consistent with local heating. For this reason we have chosen to ignore the data at times less than 20 ns in analyzing these curves.

The rate of the observed relaxation at 300 K (1/220 ns) (Figure 5) is very similar to that observed for the melting of an alanine-based peptide (1/160 ns) by Williams et al.,[6] and the rate increases monotonically with increasing temperature. In our earlier analysis, this rate was assigned to the melting and reforming of helical sequences that requires crossing of the nucleation free energy barrier.[9] There are no previous data on the temperature dependence of this process for peptides of comparable length in aqueous solvents. The monotonic temperature dependence which we observe is in marked contrast to the prediction of the Schwartz model that the slow rate should

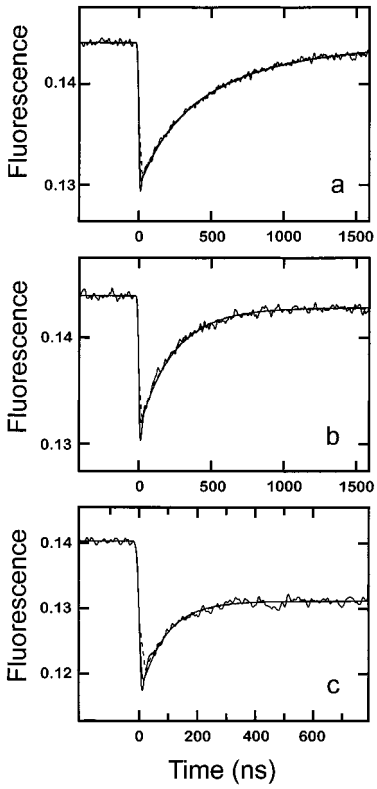

Figure 4. Kinetics for the change in fluorescence of W_1H_5-21. Data are shown for temperature jumps (a) from 269 to 281 K, (b) from 289 to 306 K and (c) from 306 to 318 K. Intensity is plotted in arbitrary units. (—) Fits to the data with the model of Muñoz et al.[1] using the parameters in Table 1. (— — —) Fits to the data with a single-exponential relaxation. The relaxation rates obtained from the fits were (a) 2.3×10^6 s^{-1}; (b) 4.3×10^6 s^{-1}; and (c) 1.0×10^7 s^{-1}.

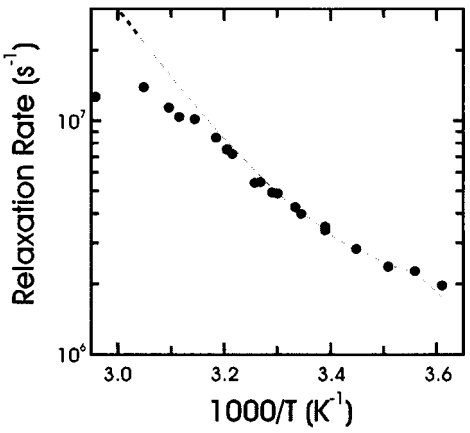

Figure 5. Temperature dependence of the relaxation rates. (●) Measured rates for the change in fluorescence of W_1H_5-21. (— — —) Slow relaxation rate obtained from a two-exponential fit to the decay of the population of species in which both W_1 and H_5^+ are helical $\{i \leq 2; i + j \geq 6\}$ predicted by the model.

exhibit a minimum near the midpoint of the melting curve.[13] Such a dependence has been observed for poly-*N*-(3−hydroxypropyl)-L-glutamine in methanol/water mixtures by Gruenewald et al.[14]

To model the kinetic data, we used the results of the equilibrium analysis described above to calculate the distribution of species at the initial temperature for each kinetic experiment. We then integrated the kinetic equations for the model at each final temperature using trial values of k_0, the intrinsic rate for the propagation reaction, and E_0, the energy barrier. This procedure was then iterated, adjusting the two kinetic parameters to obtain a best fit to the kinetic data. Because the amplitudes in these data varied somewhat from experiment to experiment, presumably as a result of changes in instrument alignment, we chose not to constrain the amplitudes to precisely match those predicted by the equilibrium data and instead allowed the amplitudes required to fit the kinetic data to be independently optimized in the fit. The fits to the data, shown in Figure 4, are excellent, with residuals which are comparable to those from the exponential fits at temperatures below 312 K. There are small but noticeable deviations at higher temperatures, where the model predicts kinetics faster than the observed relaxation. These deviations may reflect the temperature dependence of some of the model parameters which have been assumed to be temperature-independent. It is likely that they occur primarily at high temperature because the amplitudes of the fitted kinetic curves become significantly smaller at these temperatures (Figure 5b) and, in fitting the model to all of the kinetic data simultaneously, parameters are selected which optimize the fits to the progress curves at low temperatures because they have the largest amplitudes.

TABLE 2: Effects of Transition State and Viscosity Dependence on Kinetic Parameters

transition state				k_0	E_0	$\tau_{300\ K}$[a]
λ_S	λ_H	λ_G	κ	(ps^{-1})	(kcal mol^{-1})	(ns)
1	0	0	1	1.20	3.71	0.42
0.5	0	0	1	0.96	3.88	0.39
0.5	0.5	0.5	1	1.31	4.51	0.35
1	0	0	0.7	5.30	4.47	0.34
0.5	0	0	0.7	7.49	4.98	0.31
0.5	0.5	0.5	0.7	12.10	5.70	0.28

[a] Relaxation time for equilibration of the $c \rightleftarrows h$ transition calculated from the sum of the rates in eqs 12 and 13.

The parameters obtained from the fit to the kinetics are included in Table 2. In Figure 5 we compare the relaxation times obtained from single-exponential fits to the individual kinetic experiments with the average relaxation time obtained from the integrated relaxation kinetics calculated with the model. We have used the average relaxation time rather than a fitted value because, as discussed below, the kinetics of the $W_1-H_5^+$ peptide are characterized by more than one slow eigenvalue and, as a result, the relaxation predicted by the model is not a perfect single exponential. The agreement between the measured data and the predictions of the model using these parameters must be considered excellent. The model accounts for the temperature dependence of the relaxation times as arising from both the temperature dependence of the solvent (water) viscosity and an activation barrier for the $c \rightleftarrows h$ rates. With the full viscosity dependence in eqs 11−12 ($\kappa = 1$), an activation barrier of almost 4 kcal/mol is required to fit the data. This barrier is significantly larger than those calculated using a number of molecular mechanics force fields[31,33−38] and we will return to discuss this point in more detail below. The amplitudes predicted by the model for both the initial change in fluorescence produced by the temperature jump and the amplitude of the observed relaxation reproduce the qualitative features in the experimental data. The former result provides an important check on the accuracy of our model for the temperature dependence of the quantum yields of the helical and coil species obtained from the fit to the equilibrium fluorescence data.

Kinetics of Helix Formation. To explore the process of helix formation in more detail, we calculated the equilibration kinetics starting from the all-coil state ($j = 0$) using these model parameters. Snapshots of the populations are shown in Figure 6. The least stable species, which include the "nucleus" ($j =$

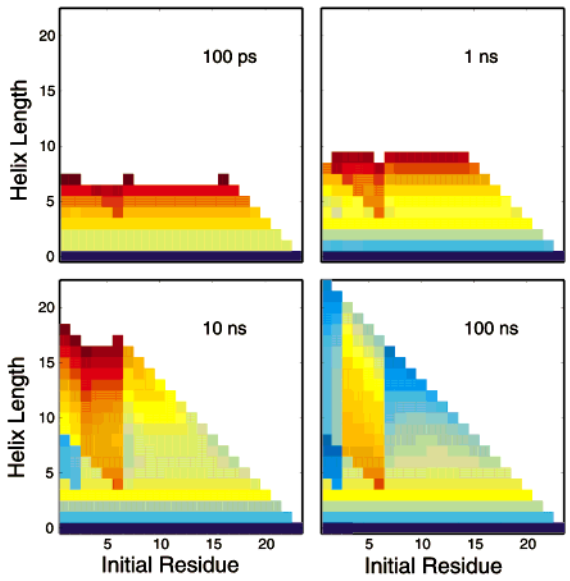

Figure 6. Time-dependent populations predicted by the model. The populations for a simulation of the helix formation kinetics of a population which is initially in the $j = 0$ (all coil) state is plotted at (a) 100 ps; (b) 1 ns; (c) 10 ns; (d) 100 ns. The populations of the 254 states of the model are represented using the same color code described in the legend to Figure 3. Species with populations less than 10^{-6} have been omitted. The number of helical residues (j) is plotted on the y axis and the initial helical residue (i) is plotted on the x axis.

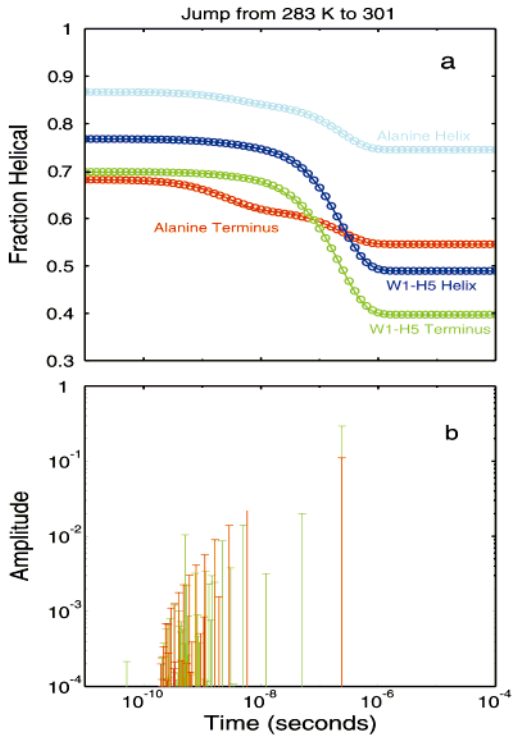

Figure 7. Comparison of temperature jump kinetics for W_1H_5-21 and a 21-residue alanine peptide at 300 K. (a) The average (red) and N-terminal (cyan) helix content of a 21-residue alanine peptide are compared with the average (blue) and N-terminal (green) helix content for W_1H_5-21. The N-terminal helix content is calculated as the sum of the populations $\{i \leq 2, i + j \geq 6\}$. The curves for both peptides were fitted with a sum of two exponential relaxations (solid red and cyan lines). For the N-terminal helix content of the alanine peptide the relaxation times are 3.5×10^8 and 4.4×10^6 s^{-1} and the amplitudes are roughly equal, 0.062 and 0.074. For the average helix content the rates are very similar, 2.7×10^8 and 4.2×10^6 s^{-1}, but the amplitude of the slow relaxation (0.097) is nearly 4 times larger than that of the fast relaxation (0.024). For the N-terminal helix content of W_1H_5-21 the relaxation rates are 8.7×10^7 and 4.5×10^6 s^{-1} but the amplitude of the slow component is 0.29, more than 20 times larger than that of the fast component (0.013). For the average helix content the rates are 4.0×10^8 and 4.2×10^6 s^{-1} and the amplitude of the slow relaxation (0.268) is 25 times larger than that of the fast relaxation (0.010). The fits to the average helix content, which show rms deviations of less than 0.1%, are better than those to the N-terminal helix content which show rms deviations which are about 3 times larger. (b) Amplitudes of eigenvectors which determine the average helix content. The amplitude of each eigenvector is plotted at the relaxation time of its eigenvalue. The amplitudes for W_1H_5-21 are shown in green and the amplitudes for the alanine peptide are shown in red.

3), reach their steady-state values within about 1 ns. It takes much longer for the populations of the longer helical states to approach their equilibrium distribution. At 100 ns, a time when a significant fraction of the final number of helical residues has been formed, the {7,17} species has the largest population, and the distribution is biased toward smaller helical species ($i \geq 7$, $j \leq 17$). Examination of the eigenvalues and eigenvectors shows that the second nonzero eigenvalue ($\tau = 50$ ns) corresponds to equilibration of this population ($i \geq 7$, $j \leq 17$) with the population having $i \leq 2$, which are stabilized by the $W_1-H_5^+$ interaction. The rate at which these species equilibrate (1/50 ns) is slowed by both the unfavorable $H_5^+-R_9^+$ interaction and the low helix propensity of H_5^+. At times significantly longer than 50 ns, the system equilibrates by converting the all-coil species to an equilibrium distribution of helical species.[39] These results point out that it is not the time required to *form* the nucleating species which limits the rate of helix formation, but the fact that the *flux* of molecules through this high free energy state is limited by its low population. This is precisely what is assumed in transition state theory: the reactant and transition state species are assumed to equilibrate instantaneously relative to the time required for product formation. The kinetics of our peptide differ from a simple two-state picture because the nucleated species require a significant fraction of the overall reaction time to equilibrate on the helical side of the barrier. All product states are thus not equilibrating rapidly on the time scale of the overall reaction.

The slow exchange between helical species in the $i \leq 2$ basin (which include the $W_1-H_5^+$ interaction) and those in the $i > 6$ basin (without the $W_1-H_5^+$ interaction) rationalizes two other interesting features of the populations shown in Figure 6. First, it is responsible for the absence of observable fast amplitude in the response to a temperature jump monitored by the fluorescence of W_1. Unzipping of the N-terminus of conformations in which W_1 is helical can only occur by breaking the favorable $W_1-H_5^+$ interaction, which slows the $h \rightarrow c$ rate, and also produces species which are destabilized by the unfavorable $H_5^+-R_9^+$ interaction. Consequently, unzipping of the N-terminus occurs primarily by exchange between the $i \leq 2$ and the $i \geq 6$ basin and is slow. Second, it results in the population of intermediate species being kinetically determined early in the reaction. At 100 ns the $i \leq 2$ states, which are stabilized by the $W_1-H_5^+$ interaction, are the most populated (Figure 6d) as they are at equilibrium (Figure 3). At shorter times, however, the population of helical species with $i \leq 6$ is very low (Figure 6b,c). The low population results from the fact that the low helix propensities of W_1 and H_5^+ not only increase the nucleation barrier but also decrease the rate of the $c \rightarrow h$ transition for these residues, so the population of nucleated species with $i \leq 6$ is kinetically "starved" at short times. Nucleation in the alanine-rich C-terminal end of the peptide produces the majority of the helical sequences.

Figure 7b shows that, despite the rather complex kinetics of helix formation, the average helical content in this simulation

is almost perfectly exponential. The reason for this result is that, while the kinetics of the population of helical species is biphasic, with a small fast phase and a large slow phase, the average helix lengths in the species which appear early in the time course are short compared to those which are present at equilibrium. As a result, the fast process is not easily seen when observing a probe of the average helix content, such as CD or IR absorption, and the time dependence of the average helix content is much closer to exponential than is that of the population of any individual species.

The "Zipping" Time. A fundamental time in our model is that required for an alanine residue at the end of a helical sequence to equilibrate between the *h* and *c* states, which we refer to as the zipping time. The reciprocal of this time determines the effective diffusion coefficient for elongation of the helical sequence. This time is of interest for several reasons. First, it can be calculated using molecular dynamics methods[31] and so can serve as a benchmark for judging the accuracy of rates obtained from dynamics simulations. Second, it can be viewed as one of the fundamental time scales in protein folding, since the time required for individual residues to diffuse in conformation space must also be closely related to this time. While this rate is, in principle, observable from infrared absorption experiments with picosecond resolution, such experiments have not yet been undertaken. We obtain indirect information about this time from modeling our experiments.

To determine how this time depends on the choice of transition state, we chose several values for the parameters λ_S, λ_H, and λ_G which specify the thermodynamic properties of the transition states for the c $\rightleftarrows$ h transitions and refitted the kinetic data. One choice is the transition state used by Muñoz et al.[1] in which the conformational entropy is completely lost but no interactions are formed. As alternative choices we picked a transition state in which only half of the entropy is lost and one which lies thermodynamically midway between the *c* and *h* states. To determine how this rate depends on the choice of the viscosity prefactor (eqs 11 and 12) we also carried out these fits using two different values for the exponent, κ; one is the standard assumption ($\kappa = 1.0$) and the other, which is based on work on the dependence of these kinetics on solution viscosity carried out by Jas et al.,[40] is a reduced value of the viscosity exponent ($\kappa = 0.7$). The kinetic parameters obtained from these six fits are summarized in Table 2. The interesting result is that the zipping time is rather independent of these assumptions. The value of $\tau_{300\ K}$ varies by only about 20% for the three transition states and by only a similar amount when the viscosity exponent, κ, is varied. The values of k_0 and E_0 produced by the fit largely compensate for the differences in the equilibrium contribution to the free energy barrier and the viscosity dependence. Within the confines of our model, we can therefore set the relaxation time for this process as approximately 0.3 ns. Because the model localizes most of the large apparent activation energy observed in Figure 5a data in these rates, this time increases to about 1.5 ns at 273 K and decreases to 20−30 ps at 373 K.

It is interesting to compare this result with the times obtained from recent molecular dynamics simulations. Brooks and coworkers have investigated the free energy surfaces for this process at 300 K using umbrella sampling.[31,34] These authors found that the barriers between these conformations had free energy maxima at values of ψ of about 45° and −120°. The smaller barrier at 45° had magnitudes relative to the helical minimum of 2−3 kcal/mol at both ends of the helix, whereas the free energy of the coil conformation was 0.5−1.5 kcal/mol less stable than that of the helix at the N-terminus of the helix and about 0.5 kcal/mol more stable at the C-terminus. They also found that longer helices were stabilized relative to short helices by the electrostatic interactions which are conventionally described as "helix dipole" effects. Based on these values, Young and Brooks[31] used the expression

$$k = \nu \exp(-W^{\ddagger}/RT) \tag{13}$$

with an assumed prefactor of $\upsilon = 10^{12}$, to estimate relaxation rates of about 1/75 ps at the C-terminus and >1/25 ps at the N-terminus of a 15-residue alanine peptide. These estimates are almost an order of magnitude faster than ours. The rates for this fundamental equilibration step in other simulations have also been calculated to be significantly faster than those we estimate from our model.[33−38] On the other hand, Mohanty et al.[41] simulated the formation of a reverse turn in the peptide SYPFDV which is limited by the rotation of the ψ dihedral angle of Y_2 of this peptide and report relaxation times of ∼0.5 to 0.7 ns at 300 K (90−160 ps at 500 K). In a recent calculation on a 16-residue peptide in which averaged solvent effects were included in the potential function and were updated at subpicosecond intervals, folding of the peptide was observed in about 3 ns, about 100 times faster than is observed experimentally.[42] It is likely that the absence of solvent friction is one factor responsible for the rapid folding observed in this simulation.

Comparison with Experiments on Other Peptides. At this point it is important to ask the question: What do we learn about other helical peptides from this study? Does W_1H_5-21, which was synthesized to provide a convenient probe of helix formation, provide more general information about the helix-coil transition? To address this question, we simulated the kinetics of a peptide of the same length in which both the tryptophan and the histidine are replaced by alanine residues. In this simulation, as in our fit to the data for W_1H_5-21, we ignore the slight difference between the helix propensity for alanine and arginine. Our simulation therefore treats the peptide as a simple homopolymer of alanine. In Figure 7 we compare temperature jump simulations for the alanine peptide with those for W_1H_5-21 at a final temperature of 300 K. With our parameters, the slowest relaxation occurs with almost the same (1/220 ns) rate in both peptides and this rate is essentially the same as that measured by Williams et al.[6] for the alanine peptide at 301 K (1/160 ns). As discussed above, the relaxation of both the average helix content and the N-terminal helix content of W_1H_5-21 can be well approximated as single-exponential relaxations with relaxation times of about 220 ns. If the calculated relaxations are fitted as the sums of two exponentials, less than 5% of the amplitude for the average helix content is found in a relaxation which is nearly 100-fold faster (2.5 ns). For the N-terminal helix content, a similar fraction of the amplitude is found in a relaxation which is about 20 times faster (12 ns). For the alanine peptide the amplitudes of the faster process are much larger. For the average helix content, about 20% of the amplitude is associated with a relaxation which is about 60 times faster (4 ns), while for the N-terminal helix content almost 50% of the amplitude is associated with this fast relaxation. This result is consistent with that predicted earlier by Thompson et al.;[9] the faster process is associated with the redistribution of helix lengths in peptides which contain a segment of α-helix. The larger amplitudes result from the fact that unzipping of the ends of the homopolymer sequence can occur without breaking any stabilizing side chain interactions. The amplitudes predicted for the alanine peptide suggest that the relaxation time for this "unzipping" process should be

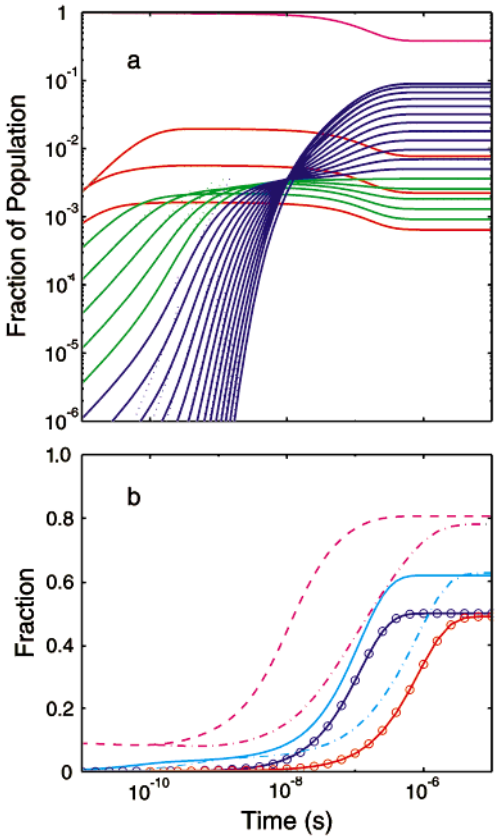

Figure 8. Coil → helix kinetics of a 21-residue alanine peptide. The kinetics were calculated using the parameters in Table 1 at the midpoint of the calculated melting transition (318 K). (a) Populations of species with j helical residues. The all-coil species ($j = 0$) is plotted in cyan. The least populated species ($j = 1{:}3$) are plotted in red; species with intermediate populations ($j = 4{:}9$) are plotted in green and the most populated species ($j = 10{:}22$) are plotted in blue. The dotted lines show the maximum slopes of each curve. The maximum slopes for species 5:22 are 1.03, 1.17, 1.40, 1.70, 2.05, 2.44, 2.84, 3.27, 3.71, 4.16, 4.61, 5.10, 5.56, 6.04, 6.56, 7.06, 7.57, and 8.23. (b) Average and N-terminal helix content. The average helix content of the peptide (blue circles) is almost perfectly exponential. The fit to a single exponential is shown as the solid blue line. The rms residual is 0.0008, only slightly greater than 1 part in 1000. The population of helix-containing species is shown in cyan, and the average fraction of residues which are helical in each helix-containing species is shown in magenta. The average helix content from a simulation at the melting temperature of W_1H_5-21 (301 K) is shown as the red circles and the single-exponential fit as the red line. The dashed cyan and magenta lines show the fraction of helix-containing species and the average fraction of helical residues, respectively.

measurable in temperature jump experiments which monitor the average helix content by infrared absorption or Raman scattering with subnanosecond time resolution or by using an N-terminal probe which does not interact strongly with its neighbors in the helix.

In Figure 8 we explore the folding kinetics of the alanine peptide in more detail. The total population of species with j helical residues has been calculated from a simulation at the melting temperature of this peptide (318 K) in which all of the population is initially in the all-coil ($j = 0$) state. For this peptide it is appropriate to sum the distributions over the initial residue, i, because the kinetics are nearly independent of i. There are several noteworthy features. First, formation of the steady-state nucleus population is one of the fastest relaxations in the population dynamics. The nuclei ($j = 3$) are the fastest species to equilibrate with the all-coil state, reaching their steady-state values in less than 100 ps. The $j = 2$ and $j = 1$ species also equilibrate within the first 200−300 ps. This result is easy to understand. Despite the fact that the $c \rightarrow h$ rate for each of these steps is only 2×10^9 s^{-1}, these steps are thermodynamically unfavorable, so the reverse rate for each step is 7×10^9 s^{-1}. The relaxation time for $j = 1$ is thus slightly more than 100 ps. The $j = 2$ and $j = 3$ species equilibrate somewhat more rapidly because they are even less stable than the $j = 1$ species and less flux is required to populate these species to their stationary levels. This result is consistent with the populations calculated for W_1H_5-21 shown in Figure 6. Once these species have equilibrated there is a constant flux of molecules into the $j = 4$ species until the all-coil state begins to decrease in population at about 10 ns. The $j \geq 4$ species grow by adding helical residues, producing a sharp "front" in the population gradient during this time interval. The species $5 \leq j \leq 22$ exhibit power-law time dependence reminiscent of the t^n dependence expected for n-step reversible sequential reactions.[43,44] The initial slopes increase monotonically from $n \simeq 1$ for $j = 5$ to $n \simeq 8$ for $j = 22$. The sharpness of this front is probably exaggerated by the use of the single sequence approximation.

To compare our kinetic results with the unfolding simulations of a 13-residue alanine peptide carried out by Daggett and Levitt,[36] we have used our model parameters (Table 2) to calculate the relaxation time for unfolding of this peptide at the elevated temperatures where unfolding was observed in their dynamics simulations. In a single trajectory at 373 K, they observed about a 30% decrease in helix content during the first 150 ps of the simulation, followed by a decrease to near 0 in the next 50 ps. Using the parameters in Table 1, we calculate a relaxation time of 700 ps at this temperature, about a factor of 3 longer than the melting time observed in this trajectory. In the absence of multiple simulated trajectories which would provide a more accurate estimate of the rate, our tentative conclusion is that the agreement between experiment and simulation is good. In more recent simulations of the helices of myoglobin, Hirst and Brooks[38] saw fraying of the C-terminal ends of the less stable helices (B, E, and F) during 1 ns simulations at 368 K. At 300 K the C-terminal end of our peptide equilibrates with shorter helical species in 2−5 ns. The fundamental rates increase by about a factor of 10 at 368 K, so we estimate relaxation times of 200−500 ps for equilibration of C-terminal alanine residues. Because of their reduced helix propensities, rates for other helix-forming residues will be somewhat slower in the absence of interactions. Nonetheless, the relatively good agreement between these two times suggests that the discrepancy between the $c \rightleftarrows h$ rates calculated from our model and those calculated by Young and Brooks[31] may result not from the calculated potential of mean force, but from the use of eq 13 to calculate the rates. A more reasonable approach might be to use the Kramers expression and estimates of the frequencies obtained from analysis of their constrained dynamics trajectories.

Comment on the Temperature Dependence of the Helix ⇄ Coil Kinetics. A surprising result of this study is the temperature dependence of the relaxation times (Figure 5). Not only is the apparent activation energy of 8 kcal/mol large but the values of E_0 in Table 2, obtained after including the temperature dependence of the solvent viscosity in the model, are also significantly larger than the calculated free energy barriers for the $c \rightleftarrows h$ transition.[31,33] Within the confines of our model we have no alternative but to put the temperature dependence into the fundamental $c \rightarrow h$ rates, but it is important to realize that this constraint is model dependent. An alternative possibility is that the observed temperature-dependent relaxation

time arises not from the propagation rates but from the barrier produced by the nucleation of helical sequences. If one were to propose a model in which the enthalpy of the $j = 3$ species was elevated by 2−3 kcal/mol relative to the $j = 0$ species, the equilibrium enthalpy difference would produce an apparent activation barrier for the folding kinetics. One set of interactions in the $j = 3$ species (nucleus) that could produce such an enthalpy change is that between peptide dipoles. Until the first turn of the helix is formed, these dipoles are arrayed pointing along the helix axis, while most of their displacement is in the plane perpendicular to this axis. The dipole−dipole interactions in this geometry are repulsive, and this repulsion increases the energy of the nucleus both relative to the $j = 0$ species and relative to longer helical species in which the peptide dipoles interact favorably with the helix dipole. While other contributions, such as side chain interactions cannot be ruled out, we are currently considering models which include an empirical parametrization of these electrostatic interactions. The equilibrium differences in such a model should be detectable in studies of the length dependence of the melting curves of helix-forming peptides since the propagation equilibrium constant becomes dependent on helix length. There are also large kinetic differences in such a model. The overall time for helix formation will exhibit significant temperature dependence whereas the ($c \rightleftarrows h$) equilibration times would become less temperature-dependent. The clearest evidence might therefore come from experiments with improved time resolution where these rates can be directly observed.

Conclusions

We have explored the helix-coil kinetics of an alanine peptide using tryptophan as a probe and modeled the kinetics using a statistical mechanical model for the helix-coil kinetics of heteropeptides. The results are extremely encouraging. The data are well fitted as single-exponential decays and the relaxation times are unexpectedly quite temperature-dependent. Using reasonable parameter values, we are able to fit all of our data and successfully predict the result that most of the amplitude is observed for the slow phase. The apparently simple kinetics seen by the $W_1-H_5^+$ fluorescence probe result from the barrier to unzipping produced by the low helix propensities and the significant stabilizing interaction of W_1 and H_5^+. These features produce a "bump" in the free energy landscape for the folded states of these peptides which impedes the unzipping of helical sequences which begin at the N-terminus. By introducing viscosity dependence and an activation barrier for helix propagation, we are not only able to quantitatively fit the experimental results but also to consistently reproduce the dynamics observed for other peptides, both in experiments and in molecular dynamics simulations. The apparently more complex dynamics of the helical states of alanine peptides are the consequence of a much flatter free energy landscape.

The ability of this relatively simple kinetic model to predict the helix−coil kinetics of these peptides holds promise for the prospect of developing a general understanding of the dynamics of this process. This study points out several issues which are of immediate importance. One is the viscosity dependence which we have already begun to investigate.[40] A second is the dependence of the kinetics and equilibria on peptide length. The length dependence should provide a clue to the source of the apparent activation barrier. A third is the question of whether this apparent success can be repeated with peptides of more varied sequence.

References and Notes

(1) Muñoz, V.; Henry, E. R.; Hofrichter, J.; Eaton, W. A. *Proc. Natl. Acad. Sci. U.S.A.* **1998**, *95*, 5872−5879.
(2) Marqusee, S., Robbins, V. H., Baldwin, R. L. *Proc. Natl. Acad. Sci. U.S.A.* **1989**, *86*, 5286- 5290. Chakrabartty, A.; Baldwin, R. L. *Adv. Protein Chem.* **1995**, *46*, 141−176.
(3) Muñoz, V.; Serrano, L. *Curr. Opin. Biotechnol.* **1995**, *6*, 382−386.
(4) Muñoz, V.; Serrano, L. *J. Mol. Biol.* **1995**, *245*, 275−296.
(5) Serrano, L. *Adv. Protein Chem.*, in press.
(6) Williams, S.; Causgrove, T. P.; Gilmanshin, R.; Fang, K. S.; Callender, R. H.; Woodruff, W. H.; Dyer, R. B. *Biochemistry* **1996**, *35*, 691.
(7) Ballew, R. M.; Sabelko, J.; Grubele, M. *Proc. Natl. Acad. Sci. U.S.A.* **1996**, *93*, 5759−5764. Ballew, R. M.; Sabelko, J.; Reiner, C.; Grubele, M. *Rev. Sci. Instrum.* **1996**, *67*, 3694−3699.
(8) Thompson, P. A. In *Techniques in Protein Chemistry*; Marshak, D. R., Ed.; Academic Press: San Diego, CA, 1997; pp 735−743.
(9) Thompson, P. A.; Eaton, W. A.; Hofrichter, J. *Biochemistry* **1997**, *36*, 9200.
(10) Schellman, J. A. *J. Phys. Chem.* **1958**, *62*, 1485−1494.
(11) Zimm, B. H.; Bragg, J. K. *J. Chem. Phys.* **1959**, *31*, 526−535.
(12) Lifson, S.; Roig, A. *J. Chem. Phys.* **1961**, *34*, 1963−1974.
(13) Schwarz, G. *J. Mol. Biol.* **1965**, *11*, 64−77.
(14) Gruenewald, B.; Nicola, C. U.; Lustig, A.; Schwarz, G.; Klump, H. *Biophys. Chem.* **1979**, *9*, 137−147.
(15) Shoemaker, K. R.; Fairman, R.; Schultz, D. A.; Robertson, A. D.; York, E. J.; Stewart, J. M.; Baldwin, R. L. *Biopolymers* **1990**, *29*, 1−11.
(16) Fernandez-Recio, J.; Vasquez, A.; Civera, C.; Sevilla, P.; Sancho, J. *J. Mol. Biol.* **1997**, *267*, 184−197.
(17) Shinitizky, M.; Goldman, R. *Eur. J. Biochem.* **1967**, *3*, 129−144.
(18) Steiner, R.; Kirby, E. P. *J. Phys. Chem.* **1969**, *73*, 4130−4135.
(19) Gill, S. C.; von Hippel, P. H. *Anal. Biochem.* **1989**, *182*, 319−326.
(20) Scholtz, J. M.; Qian, H.; York, E. J.; Stewart, J. M.; Baldwin, R. L. *Biopolymers* **1991**, *31*, 1463−1470.
(21) Chakrabartty, A.; Kortemme, T.; Padmanabhan, S.; Baldwin, R. L. *Biochemistry* **1993**, *32*, 5560−5563.
(22) Tinoco, I.; Woody, R. W.; Bradley,. D. F. *J. Chem Phys.* **1963**, *38*, 1317−1325.
(23) Madison, V.; Schellman, J. *Biopolymers* **1972**, *11*, 1041−1076.
(24) Manning, M. C.; Woody, R. W. *Biopolymers* **1991**, *31*: 569−586.
(25) Chen, T.-H.; Yang, J. T.; Chau, K. H. *Biochemistry* **1974**, *13*, 3350−3359.
(26) Much of this work is summarized in *Circular Dichroism and the Conformational Analysis of Biomolecules*; Fasman, G. D., Ed; (Plenum Press: New York, 1996) particularly in the chapters: *Theory of Circular Dichroism of Proteins*, by R. W. Woody); *Determination of Protein Secondary Structure*, by S. Y. Venyaminov and J. T. Yang; *Aromatic and Cystine Side Chain Circular Dichroism of Proteins*, by R. W. Woody and A. K. Dunker, and *CD Spectroscopy and the Helix-Coil Transition in Peptides and Polypeptides*, by N. R. Kallenbach, P. Lyu and H. Zhou.
(27) Robbins, B. J.; Fleming, G. R.; Beddard, G. S.; Robinson, G. W.; Thistlethwaite, P. J.; Woolfe, G. J. *J. Am. Chem Soc.* **1980**, *102*, 6271−6279.
(28) Preliminary lifetime studies of our control peptides have shown that the fluorescence decay is biphasic with a minor fast (∼2 ns) component which accounts for approximately 20% of the amplitude (Thompson et al., unpublished work). Our simplified model for tryptophan quenching describes the decay of the singlet state by a single-exponential relaxation, and so cannot provide an accurate description of the quenching of these peptides. Since our analysis of the intensities is only approximate, we have nonetheless used eq 7 to fit the quantum yields of both the control peptides and the helical and nonhelical forms of W_1H_5-21.
(29) Muñoz, V.; Thompson, P. A.; Hofrichter, J.; Eaton, W. A. *Nature* **1997**, *390*, 196−199.
(30) While the model could, in principle, also incorporate a number of other contributions to helix stability, such as the effects of capping and charge−dipole interactions, our database at this time is too limited to permit us to evaluate such effects.
(31) Young, W. S.; Brooks, C. L. *J. Mol. Biol.* **1996**, *259*, 560−572.
(32) Loewenthal, R.; Sancho, J.; Ferscht, A. R. *J. Mol. Biol.* **1992**, *224*, 759−770.
(33) Anderson, A. G.; Hermans, J. *Proteins* **1988**, *3*, 262−265.
(34) Tobias, D. J.; Brooks, C. L. *Biochemistry* **1991**, *30*, 6059−6070.
(35) Soman, K. V.; Karimi, A.; Case, D. A. *Biopolymers* **1991**, *31*, 1351−1361.
(36) Daggett, V.; Levitt, M. *J. Mol. Biol.* **1992**, *223*, 1121−1138.
(37) Brooks, C. L.; Case, D. A. *Chem. Rev.* **1993**, *93*, 2487−2502.
(38) Hirst, J. D.; Brooks, C. L. *Biochemistry* **1995**, *34*, 7614−7621.
(39) Clarke et al. (*Proc. Natl. Acad. Sci. U.S.A.* **1999**, *96*, 7232−7237) have reported that the formation of helix in a 16-residue alanine peptide,

solubilized by lysine side chains, occurs on the 100 ms time scale, as monitored by stopped-flow CD measurements. We have looked at the folding of W_1H_5-21 in stopped flow experiments in which the peptide was diluted from 5 M GdnHCl, pH 4.8, 0.2 M GdnHCl, pH 4.8, at room temperature. The change in fluorescence was >95% complete within 3 ms, which we estimate as the "dead time" of our stopped-flow instrument. In data collected under slightly different conditions, we have also verified that, to within the experimental uncertainty of ~5%, the entire change in fluorescence amplitude observed in equilibrium experiments occurs in the relaxations shown in Figure 4. We therefore conclude that there is no slow amplitude in the folding of W_1H_5-21 which can be detected using our fluorescence probe, as expected from our model.

(40) Jas, G. S., et al. (Manuscript in preparation).

(41) Mohanty, D.; Elber, R.; Thirumalai, D.; Beglov, D.; Roux, B. *J. Mol. Biol*. **1997**, *272*, 423−442.

(42) Sung, S.-S.; Wu, X.-W. *Biopolymers* **1997**, *42*, 633−644.

(43) Abraham, F. F. *J. Chem. Phys*. **1969**, *51*, 1632−1638.

(44) Hofrichter, J.; Ross, P. D.; Eaton, W. A. *Proc. Natl. Acad. Sci. U.S.A.* **1974**, *71*, 4864−4868.